Potassium-Ion Batteries

International Edition: DOI: 10.1002/anie.201908607
German Edition: DOI: 10.1002/ange.201908607

Electrolyte Chemistry Enables Simultaneous Stabilization of Potassium Metal and Alloying Anode for Potassium-Ion Batteries

*Hua Wang[+], Dandan Yu[+], Xiao Wang, Zhiqiang Niu, Mengxue Chen, Liwei Cheng, Wei Zhou, and Lin Guo**

Abstract: *Alloying anodes are promising high-capacity electrode materials for K-ion batteries (KIBs). However, KIBs based on alloying anodes suffer from rapid capacity decay due to the instability of K metal and large volume expansion of alloying anodes. Herein, the effects of salts and solvents on the cycling stability of KIBs based on a typical alloying anode such as amorphous red phosphorus (RP) are investigated, and the potassium bis(fluorosulfonyl)imide (KFSI) salt-based carbonate electrolyte is versatile to achieve simultaneous stabilization of K metal and RP electrodes for highly stable KIBs. This salt-solvent complex with a moderate solvation energy can alleviate side reactions between K metal and the electrolyte and facilitate K^+ ion diffusion/desolvation. Moreover, robust SEI layers that form on K metal and RP electrodes can suppress K dendrite growth and resist RP volume change. This strategy of electrolyte regulation can be applicable to other alloying anodes for high-performance KIBs.*

Potassium-ion batteries (KIBs) have emerged as an alternative to lithium-ion batteries for large-scale energy storage due to their low redox potential and abundant potassium resources.[1] Generally, alloying anodes such as tin (Sn), phosphorus (P), antimony (Sb), bismuth (Bi), and Sn_4P_3 that work via the alloying-dealloying mechanism are regarded as appealing electrode materials for high-performance KIBs (Figure 1 A).[2–10] However, KIBs based on alloying anodes deliver unsatisfactory fast capacity decay during cycling. On the one hand, large volume change of alloying anodes during potassiation and depotassiation leads to solid-electrolyte interphase (SEI) rupture and material pulverization.[5a–c,10] This induces continual electrolyte consumption and severely lessens the electrical connection between active particles.[4b,5a,8a] On the other hand, potassium metal suffers from undesirable degradation during cycling owing to the unstable SEI formation and poor reversibility of potassium plating/stripping.[5d] Moreover, potential potassium dendrite growth will cause detrimental side reactions and electrolyte decomposition, caused by the high chemical reactivity of potassium.[4a,11a] Consequently, simultaneous alleviation of the large volume change in the alloying anode and passivation of potassium metal is a major challenge that has to be solved to prolong the lifespan of KIBs.

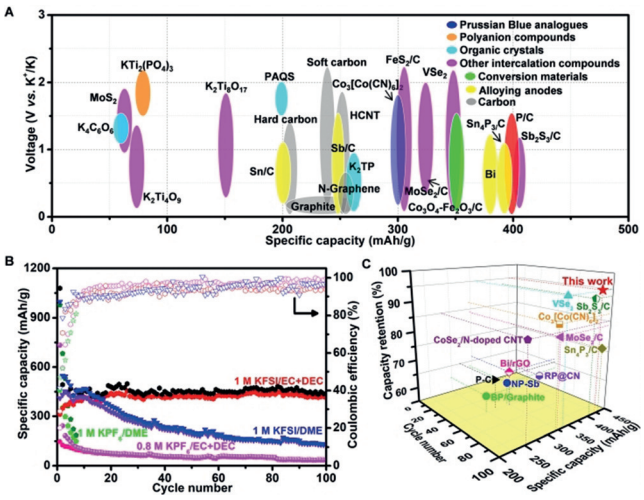

Figure 1. (A) Capacity vs. voltage plots of anodes for KIBs reported to date. (B) Cycling performance curves of KIBs based on RP/C alloying anodes with different electrolytes at 50 $mA\,g^{-1}$. (C) Comparison of the cycling stability of RP/C electrodes with various previously reported anodes for KIBs. Current density: 50 mA/g-black P (BP)/graphite,[7a] amorphous black P/carbon (P-C),[8a] Sn_4P_3@carbon fibers (Sn_4P_3/C),[4a] Bi/rGO[5a] and RP/C (this work); 100 mA/g-RP@carbon nanosheet (RP@CN),[9] nanoporous Sb (NP-Sb)[12] and cobalt hexacyanocobaltate ($Co_3[Co(CN)_6]_2$);[6b] 200 mA/g-VSe_2,[3a] $MoSe_2$/C[3b] and $CoSe_2$/N-doped CNT;[16] 500 mA/g-antimony sulfide/carbon sheet (Sb_2S_3/C).[6a] The specific capacity of RP@CN and Sn_4P_3/C was given based on the mass of phosphorus-based active materials.

To promote cyclability of alloying anodes for KIBs, great efforts have been devoted to designing efficient nanostructures,[12] introducing a conductive carbon matrix,[7,8] engineering of binary alloys,[4,13] and utilizing suitable electrolytes.[5] These strategies are effective in alleviating the large volume change of alloying anodes. However, the degradation of potassium metal is generally ignored during cycling, which has a great negative impact on the cycle life of KIBs.[5] It is well known that the electrolyte system plays essential roles in passivating alkali metals and manipulating the composition of SEI layers, which is expected to achieve simultaneous

[*] Dr. H. Wang,[+] D. Yu,[+] M. Chen, L. Cheng, Prof. W. Zhou, Prof. L. Guo
School of Chemistry, Beijing Advanced Innovation Center for Biomedical Engineering, Beihang University
Beijing 100191 (China)
E-mail: guolin@buaa.edu.cn
Dr. X. Wang
Department of Chemistry, Virginia Tech
Blacksburg, VA 24061 (USA)
Prof. Z. Niu
Key Laboratory of Advanced Energy Materials Chemistry of Ministry of Education, School of Chemistry, Nankai University
Tianjin 300071 (China)
[+] These authors contributed equally to this work.
Supporting information and the ORCID identification number(s) for the author(s) of this article can be found under: https://doi.org/10.1002/anie.201908607.

stabilization of potassium metal and the alloying anode.[11,14,15] Therefore, it is crucial to gain a deeper understanding of the effects of electrolyte composition on the cycling performance of KIBs based on alloying anodes.

As a typical alloying anode, amorphous red phosphorous (RP) is one of the most promising electrode materials for KIBs due to its low cost, high availability, natural abundance of phosphorous (0.1 wt% in the Earth's crust) and good chemical stability.[8–10] Herein, our work investigates the impacts of the electrolyte salt and solvent chemistry on the stability of both K metal and RP electrodes in KIBs. The potassium bis(fluorosulfonyl)imide (KFSI) salt-based carbonate electrolyte is demonstrated to be a multifunctional electrolyte to realize highly stable potassium-ion storage which exceeds that of most previously reported anodes for KIBs.

RP/carbon nanotube@reduced graphene oxide (RP/C) composites were fabricated by ultrasonic treatment and a self-assembly process. Characterization of RP/C shows that amorphous RP particles are well embedded in a three-dimensional conducting carbon network by forming P–O/P–C bonds (Figure S1–S4, Supporting Information). Electrochemical performance of KIBs based on RP/C alloying anodes was evaluated employing different electrolytes. The 1M KFSI/ethylene carbonate (EC) + diethyl carbonate (DEC) electrolyte enables superior stability for KIBs compared to the other electrolytes (Figure 1B and Figure S5–7). The reversible capacity of RP/C electrodes increases to 440.2 mAh g^{-1} in the 20th cycle due to activation and maintains at 420.7 mAh g^{-1} after 100 cycles. The specific capacity of RP in RP/C electrodes is estimated to be 590 mAh g^{-1} (Figure S8A). More importantly, the cycling stability and high capacity are superior to most of those reported for anodes for KIBs (Figure 1C). RP/C electrodes also exhibit good rate and long-term cycling performance (Figure S8B–D). These results demonstrate that electrochemical properties of KIBs based on alloying anodes can be effectively promoted by regulating the electrolyte composition.

First, the interaction between electrolyte salts and solvents was investigated by Raman spectroscopy. The peak at 718 cm^{-1} (Figure 2A) is assigned to the C=O bending of free EC molecules in hybrid EC + DEC solvents. A new peak at 729 cm^{-1} emerges in carbonate-based electrolytes and mainly originates from K^+-solvated EC.[17] Two peaks at 822 and 849 cm^{-1} (Figure 2B) can be assigned to the rocking vibration of CH_2 and stretching vibration of C–O of dimethoxyethane (DME), respectively. Similarly, two new peaks at 835 and 860 cm^{-1} appear for DME-based electrolytes, which are attributed to K^+-solvated DME.[18] The proportion and intensity of peaks corresponding to K^+-solvated molecules for KFSI-based electrolytes are higher than those for potassium hexafluorophosphate (KPF_6), suggesting that KFSI induces a stronger solvation.[18b] This will lower the amount of free solvent in the electrolyte, likely alleviating parasitic reactions between K metal and solvent molecules.[11]

To unveil the impacts of electrolyte chemistry on potassium metal, symmetric K/K cells were investigated. The voltage curve of the cells using 1M KFSI/EC + DEC remains steady for 100 cycles (Figure 2C), indicating the formation of stable SEI layers on potassium metal to accommodate large volume fluctuations and inhibit electrolyte decomposition. In 0.8M KPF_6/EC + DEC, the low voltage hysteresis sharply decreases after a few cycles, indicating a short circuit in the cell caused by K dendrites.[4a,19] Electrochemical impedance spectra (EIS) reveal that 1M KFSI/EC + DEC-based K/K cells exhibit constant impedance after 10 cycles, suggesting good cycling stability of the K metal. No dendrites are observed to penetrate the separator after 100 cycles (Figure 2D). In 1M KFSI/EC + DEC electrolyte, the K/K cells work efficiently even at a current density of 5 mA cm^{-2}, unlike 0.8M KPF_6/EC + DEC (Figure 2E). Nevertheless, voltage profiles of K/K cells (Figure S9) and digital photos of separators after cycling (Figure S10) confirm serious K dendrite formation in 1M KFSI/DME and poor reversibility of K plating/stripping in 1M KPF_6/DME. These results demonstrate that the utilization of 1M KFSI/EC + DEC can effectively suppress K dendrite growth and inhibit electrolyte decomposition to boost the cycling and rate performance of K metal batteries.

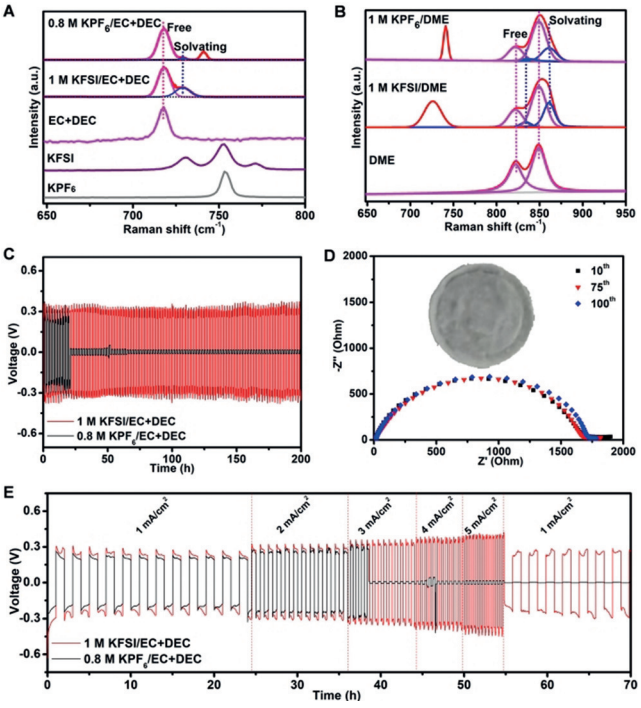

Figure 2. Raman spectra of (A) carbonate- and (B) ether-based electrolytes. (C) Voltage profiles of K plating/stripping in K/K cells with carbonate-based electrolytes at 1 mA cm^{-2} for 1 mAh cm^{-2}. (D) Nyquist plots of K/K cells with 1M KFSI/EC + DEC after selected cycles. Inset: a digital photo of the separator after 100 cycles. (E) Rate capability of K/K cells with carbonate-based electrolytes in the capacity of 1 mAh cm^{-2}.

X-ray photoelectron spectroscopy (XPS) measurements were performed to analyse the composition of SEI layers on RP/C alloying anodes (Figure 3A–C). The C 1s spectra can be split into four peaks with binding energies of 284.8 (C–C), 286.4 (C–O–C), 287.8 (C=O) and 289.5 eV (RO-COOK).[5b,d,20] In O 1s spectra, the peak at 530.3 eV is assigned to potassium salts originating from salt decomposition.[4b] Two peaks at 533.4 (RO-COOK) and 534.2 eV (ROK)

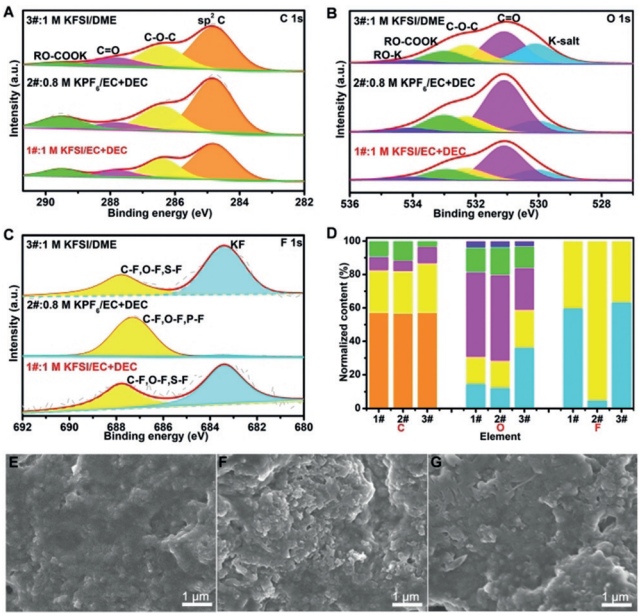

Figure 3. XPS patterns of discharged RP/C electrodes after 10 cycles at 50 mA g^{-1}. (A) C 1s, (B) O 1s, (C) F 1s, and (D) the relative content of different species in SEI layers, in which the corresponding specie is represented by the same color shown in the C 1s, O 1s and F 1s spectra, respectively. SEM images of RP/C electrodes cycled with (E) 1 M KFSI/EC + DEC, (F) 0.8 M KPF_6/EC + DEC and (G) 1 M KFSI/DME after 10 cycles.

are derived from solvent reduction. The F 1s spectra exhibit two peaks around 683.3 (K–F) and 687.4 eV (C–F, O–F, S–F or P–F).[4a,5a,11b] S 2p and N 1s spectra (Figure S11) further demonstrate salt reduction in the KFSI-based electrolyte.[11a,21] To evaluate the composition differences of SEI layers, we calculated the integral areas of individual peaks and the normalized content of each component is summarized in Figure 3D. Organic components dominate the SEI layer when using 0.8 M KPF_6/EC + DEC, while more inorganic salts are generated when utilizing 1 M KFSI/DME and 1 M KFSI/EC + DEC. Compared to organic species, inorganic salts possess better mechanical strength to accommodate large volume changes, but an excessive content of inorganic compounds will induce SEI failure during cycling.[22] Consequently, an integrated organic-inorganic SEI layer is favoured, as can be found on the RP/C alloying anode cycled in 1 M KFSI/EC + DEC.

Scanning electron microscope (SEM) images (Figure 3E–G) show a compact and uniform SEI layer formed on the RP/C electrode cycled in 1 M KFSI/EC + DEC, which is in contrast to the electrode cycled in 0.8 M KPF_6/EC + DEC. The SEI layers formed in ether-based electrolytes are thicker and denser than those formed in carbonate-based electrolytes. Severe ruptures are present when using 1 M KPF_6/DME (Figure S12). Transmission electron microscope images also indicate the integrity of the SEI layer formed in 1 M KFSI/EC + DEC (Figure S13), suggesting that the electrolyte benefits from the formation of a stable SEI layer on the RP/C alloying anode to accommodate the volume change during cycling. In addition, the final potassiation product of RP is shown to be KP (Figure S14,15).[7a,8b,9]

EIS analysis was carried out to evaluate the electrode kinetics of KIBs based on RP/C alloying anodes. The resistance of 1 M KFSI/EC + DEC-based KIBs is almost constant after 50 cycles (Figure 4A) and the charge-transfer resistance (R_{ct}) dominates the overall resistance variation (Figure 4B).[23] However, a continuous increase in resistance

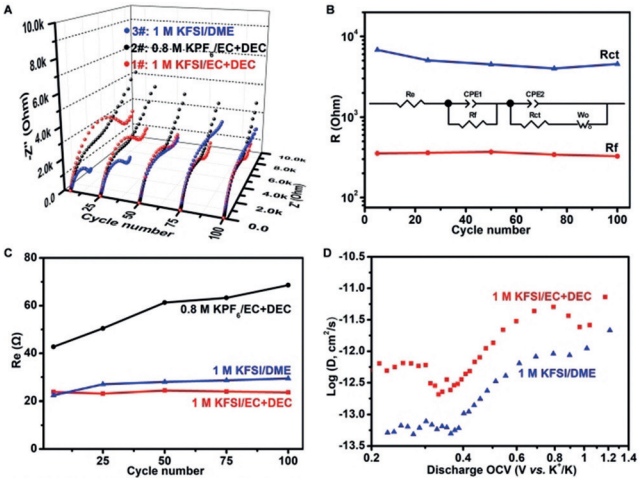

Figure 4. (A) Nyquist plots of KIBs based on RP/C alloying anodes after 5, 25, 50, 75 and 100 cycles. (B) Resistance variation curves of KIBs using 1 M KFSI/EC + DEC after selected cycles (inset: equivalent circuit). Rf: resistance from the SEI layer. (C) Re of KIBs after 5, 25, 50, 75 and 100 cycles. (D) K-ion diffusion coefficient in RP/C electrodes for KIBs cycled with 1 M KFSI/EC + DEC and 1 M KFSI/DME, respectively, at different discharged states.

can be found during cycling when using 1 M KFSI/DME. In 0.8 M KPF_6/EC + DEC, electrolyte resistance (Re) changes from 42.7 to 68.6 Ω as the cycle number increases from 5 to 100 (Figure 4C), suggesting the instability of this electrolyte in working KIBs. In addition, galvanostatic intermittent titration technique measurements (Figure 4D and Figure S16,17) reveal that the K^+ ion diffusion coefficient in 1 M KFSI/EC + DEC is higher than that in 1 M KFSI/DME. This is in agreement with the gradient of slope lines in the low-frequency region of the Nyquist plots. These findings indicate that a stable and highly K^+ ion-conductive SEI layer forms on the RP/C alloying anode when using 1 M KFSI/EC + DEC for highly stable KIBs.

Density functional theory calculations were carried out to better understand the rapid kinetics and stable SEI formation in 1 M KFSI/EC + DEC (Table S1–4 and Figure S18). The solvation energy of KFSI-based electrolytes is higher than that of KPF_6-related electrolytes, which leads to a higher degree of solvation molecules, reducing side reactions between potassium metal and electrolyte molecules (Figure 5A). Moreover, the low solvation energy of KFSI-EC/DEC (1.38 eV) compared to that of KFSI-2DME (1.53 eV) indicates a weak interaction between the salt and solvent, facilitating K^+ ion diffusion and desolvation.[13,24] In addition, the LUMO energy of K^+-EC/DEC is lower than that of K^+-2DME, which suggests the reduction of hybrid EC + DEC solvents is easier (Figure 5B).[25] Thus, more organic species are generated in SEI layers when using carbonate-based

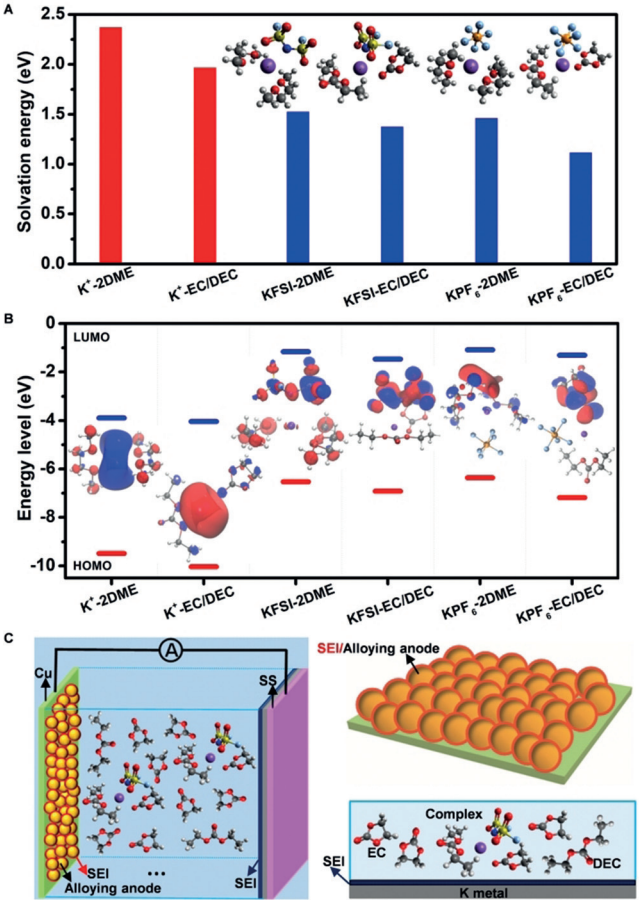

Figure 5. (A) Solvation energies and (B) highest occupied molecular orbital (HOMO)-lowest unoccupied molecular orbital (LUMO) energy levels of solvated K^+ ions and salt-solvent complexes in various electrolytes obtained by the Perdew-Burke-Ernzerhof (PBE) functional (inset: optimized geometrical structures and visual LUMOs). (C) Solvation sheath of K^+ ions and formation of stable SEI layers on both K metal and the alloying anode using 1 M KFSI/EC + DEC. Colors for different elements: H white, K purple, C gray, O red, N blue, F light blue, S yellow and P orange.

electrolytes. Taking into account the anion impact, the KFSI-EC/DEC complex has a lower LUMO energy than KPF_6-EC/DEC, confirming the reduction of KFSI is preferable to KPF_6. These results demonstrate that the salt and solvent in 1 M KFSI/EC + DEC facilitate the formation of a strong and flexible SEI layer and support K^+ ion diffusion/desolvation for better K metal protection and cycling stability of alloying anodes (Figure 5C).

In summary, K metal and alloying anodes have been simultaneously stabilized by regulating electrolyte chemistry to achieve highly stable K-ion storage. Benefiting from the KFSI-based carbonate electrolyte, KIBs based on RP/C alloying anodes deliver a high capacity of 420.7 $mAh\,g^{-1}$ after 100 cycles with a capacity retention of 95.3%, which surpasses that of most reported anodes for KIBs. The KFSI-EC/DEC complex with a moderate solvation energy can effectively decrease parasitic reactions between K metal and the electrolyte and facilitate K^+ ion diffusion and desolvation into RP/C alloying anodes.

Moreover, stable and robust SEI layers can form on potassium metal and RP/C electrodes to suppress K dendrite growth, accommodate large volume fluctuations and inhibit electrolyte decomposition, which contribute to prolonging the lifespan of KIBs. Our strategy of electrolyte optimization to simultaneously stabilize potassium metal and alloying anodes should be applicable to other advanced alkali metal battery systems based on alloying anodes.

Acknowledgements

The authors acknowledge the financial support of the National Natural Science Foundation of China (51822201, 51622204 and 51532001).

Conflict of interest

The authors declare no conflict of interest.

Keywords: alloying anode · dendrite · electrolyte · potassium metal · potassium-ion batteries

How to cite: *Angew. Chem. Int. Ed.* **2019**, *58*, 16451 – 16455
Angew. Chem. **2019**, *131*, 16603 – 16607

[1] a) T. Masese, K. Yoshii, Y. Yamaguchi, T. Okumura, Z. D. Huang, M. Kato, K. Kubota, J. Furutani, Y. Orikasa, H. Senoh, H. Sakaebe, M. Shikano, *Nat. Commun.* **2018**, *9*, 3823; b) Y.-H. Zhu, Q. Zhang, X. Yang, E.-Y. Zhao, T. Sun, X.-B. Zhang, S. Wang, X.-Q. Yu, J.-M. Yan, Q. Jiang, *Chem* **2019**, *5*, 168 – 179.

[2] a) H. Kim, J. C. Kim, M. Bianchini, D.-H. Seo, J. Rodriguez-Garcia, G. Ceder, *Adv. Energy Mater.* **2018**, *8*, 1702384; b) K. Lei, F. Li, C. Mu, J. Wang, Q. Zhao, C. Chen, J. Chen, *Energy Environ. Sci.* **2017**, *10*, 552 – 557; c) Z. Jian, W. Luo, X. Ji, *J. Am. Chem. Soc.* **2015**, *137*, 11566 – 11569.

[3] a) C. Yang, J. Feng, F. Lv, J. Zhou, C. Lin, K. Wang, Y. Zhang, Y. Yang, W. Wang, J. Li, S. Guo, *Adv. Mater.* **2018**, *30*, 1800036; b) W. Wang, B. Jiang, C. Qian, F. Lv, J. Feng, J. Zhou, K. Wang, C. Yang, Y. Yang, S. Guo, *Adv. Mater.* **2018**, *30*, 1801812.

[4] a) W. Zhang, W. K. Pang, V. Sencadas, Z. Guo, *Joule* **2018**, *2*, 1534 – 1547; b) Z. Wang, K. Dong, D. Wang, S. Luo, Y. Liu, Q. Wang, Y. Zhang, A. Hao, C. Shi, N. Zhao, *J. Mater. Chem. A* **2019**, *7*, 14309 – 14318.

[5] a) Q. Zhang, J. Mao, W. K. Pang, T. Zheng, V. Sencadas, Y. Chen, Y. Liu, Z. Guo, *Adv. Energy Mater.* **2018**, *8*, 1703288; b) J. Huang, X. Lin, H. Tan, B. Zhang, *Adv. Energy Mater.* **2018**, *8*, 1703496; c) R. Zhang, J. Bao, Y. Wang, C.-F. Sun, *Chem. Sci.* **2018**, *9*, 6193 – 6198; d) L. Madec, V. Gabaudan, G. Gachot, L. Stievano, L. Monconduit, H. Martinez, *ACS Appl. Mater. Interfaces* **2018**, *10*, 34116 – 34122.

[6] a) Y. Liu, Z. Tai, J. Zhang, W. K. Pang, Q. Zhang, H. Feng, K. Konstantinov, Z. Guo, H. K. Liu, *Nat. Commun.* **2018**, *9*, 3645; b) L. Deng, Z. Yang, L. Tan, L. Zeng, Y. Zhu, L. Guo, *Adv. Mater.* **2018**, *30*, 1802510.

[7] a) I. Sultana, M. M. Rahman, T. Ramireddy, Y. Chen, A. M. Glushenkov, *J. Mater. Chem. A* **2017**, *5*, 23506 – 23512; b) D. Liu, X. Huang, D. Qu, D. Zheng, G. Wang, J. Harris, J. Si, T. Ding, J. Chen, D. Qu, *Nano Energy* **2018**, *52*, 1 – 10; c) X.-D. He, Z.-H. Liu, J.-Y. Liao, X. Ding, Q. Hu, L.-N. Xiao, S. Wang, C.-H. Chen, *J. Mater. Chem. A* **2019**, *7*, 9629 – 9637.

[8] a) X. Wu, W. Zhao, H. Wang, X. Qi, Z. Xing, Q. Zhuang, Z. Ju, *J. Power Sources* **2018**, *378*, 460 – 467; b) W.-C. Chang, J.-H. Wu, K.-T. Chen, H.-Y. Tuan, *Adv. Sci.* **2019**, *6*, 1801354.
[9] P. Xiong, P. Bai, S. Tu, M. Cheng, J. Zhang, J. Sun, Y. Xu, *Small* **2018**, *14*, 1802140.
[10] Y. Wu, S. Hu, R. Xu, J. Wang, Z. Peng, Q. Zhang, Y. Yu, *Nano Lett.* **2019**, *19*, 1351 – 1358.
[11] a) N. Xiao, W. D. McCulloch, Y. Wu, *J. Am. Chem. Soc.* **2017**, *139*, 9475 – 9478; b) L. Lutz, D. A. D. Corte, M. Tang, E. Salager, M. Deschamps, A. Grimaud, L. Johnson, P. G. Bruce, J.-M. Tarascon, *Chem. Mater.* **2017**, *29*, 6066 – 6075.
[12] Y. An, Y. Tian, L. Ci, S. Xiong, J. Feng, Y. Qian, *ACS Nano* **2018**, *12*, 12932 – 12940.
[13] W. Zhang, Z. Wu, J. Zhang, G. Liu, N.-H. Yang, R.-S. Liu, W. K. Pang, W. Li, Z. Guo, *Nano Energy* **2018**, *53*, 967 – 974.
[14] a) X. Liang, Q. Pang, I. R. Kochetkov, M. S. Sempere, H. Huang, X. Sun, L. F. Nazar, *Nat. Energy* **2017**, *2*, 17119; b) M. D. Tikekar, S. Choudhury, Z. Tu, L. A. Archer, *Nat. Energy* **2016**, *1*, 16114.
[15] a) Y. Gao, Z. Yan, J. L. Gray, X. He, D. Wang, T. Chen, Q. Huang, Y. C. Li, H. Wang, S. H. Kim, T. E. Mallouk, D. Wang, *Nat. Mater.* **2019**, *18*, 384 – 389; b) D. Lin, Y. Liu, Y. Cui, *Nat. Nanotechnol.* **2017**, *12*, 194 – 206.
[16] Q. Yu, B. Jiang, J. Hu, C. Y. Lao, Y. Gao, P. Li, Z. Liu, G. Suo, D. He, W. A. Wang, G. Yin, *Adv. Sci.* **2018**, *5*, 1800782.
[17] a) H. Y. Song, T. Fukutsuka, K. Miyazaki, T. Abe, *Phys. Chem. Chem. Phys.* **2016**, *18*, 27486 – 27492; b) X. Gao, G. Zhu, Q. Qu, G. Liu, V. S. Battaglia, H. Zheng, *J. Electrochem. Soc.* **2018**, *165*, A3844 – A3853.
[18] a) Y. Yamada, M. Yaegashi, T. Abe, A. Yamada, *Chem. Commun.* **2013**, *49*, 11194 – 11196; b) L. Fan, R. Ma, J. Wang, H. Yang, B. Lu, *Adv. Mater.* **2018**, *30*, 1805486.
[19] B. Wu, J. Lochala, T. Taverne, J. Xiao, *Nano Energy* **2017**, *40*, 34 – 41.
[20] M. Dahbi, N. Yabuuchi, M. Fukunishi, K. Kubota, K. Chihara, K. Tokiwa, X.-F. Yu, H. Ushiyama, K. Yamashita, J.-Y. Son, Y.-T. Cui, H. Oji, S. Komaba, *Chem. Mater.* **2016**, *28*, 1625 – 1635.
[21] Q. Ma, X.-X. Zeng, J. Yue, Y.-X. Yin, T.-T. Zuo, J.-Y. Liang, Q. Deng, X.-W. Wu, Y.-G. Guo, *Adv. Energy Mater.* **2019**, *9*, 1803854.
[22] Z. Zhu, Y. Tang, Z. Lv, J. Wei, Y. Zhang, R. Wang, W. Zhang, H. Xia, M. Ge, X. Chen, *Angew. Chem. Int. Ed.* **2018**, *57*, 3656 – 3660; *Angew. Chem.* **2018**, *130*, 3718 – 3722.
[23] a) S. S. Zhang, K. Xu, T. R. Jow, *Electrochim. Acta* **2004**, *49*, 1057 – 1061; b) L. Wang, J. Yang, J. Li, T. Chen, S. Chen, Z. Wu, J. Qiu, B. Wang, P. Gao, X. Niu, H. Li, *J. Power Sources* **2019**, *409*, 24 – 30.
[24] a) X. Q. Zhang, X. Chen, X. B. Cheng, B. Q. Li, X. Shen, C. Yan, J. Q. Huang, Q. Zhang, *Angew. Chem. Int. Ed.* **2018**, *57*, 5301 – 5305; *Angew. Chem.* **2018**, *130*, 5399 – 5403; b) K. K. Lee, K. Park, H. Lee, Y. Noh, D. Kossowska, K. Kwak, M. Cho, *Nat. Commun.* **2017**, *8*, 14658.
[25] S. Jiao, X. Ren, R. Cao, M. H. Engelhard, Y. Liu, D. Hu, D. Mei, J. Zheng, W. Zhao, Q. Li, N. Liu, B. D. Adams, C. Ma, J. Liu, J.-G. Zhang, W. Xu, *Nat. Energy* **2018**, *3*, 739 – 746.

Manuscript received: July 10, 2019
Accepted manuscript online: September 4, 2019
Version of record online: September 26, 2019

